Strathprints Institutional Repository

AN UNAVERAGED COMPUTATIONAL MODEL OF A VARIABLY POLARIZED UNDULATOR FEL

L.T. Campbell and B.W.J. McNeil

SUPA, Department of Physics, University of Strathclyde, Glasgow, UK

Abstract

An unaveraged 3D model of the FEL has been developed which can model variably polarised undulators. The radiation field polarisation is self-consistently driven by the electron dynamics and is completely variable. This paper describes both physical model and computational code.

INTRODUCTION

Future FEL's may need to utilize effects which occur on the scale of a resonant radiation wavelength or smaller, timescales which are beyond the resolution of averaged FEL simulation codes. In order to investigate these effects and the facilities which will exploit them, 3D codes which solve unaveraged mathematical models of the FEL will be needed. The simulation codes of [1] and [2] are such codes. The disadvantage of a mathematical model with increased resolution is of course the much higher sampling rates needed to accurately model the system. To handle potentially very large data sizes such codes are best run in parallel on multiple processors.

In this paper the development of the unaveraged parallel computational model from [1] and [2] is reported. In [2], the variable H was added to describe the strength of the wiggler field in the x axis. This has been replaced by two new variables to control the strength of the wiggler field in both x and y enabling full variable wiggler polarization. The numerical method has been further refined to enhance its speed returning to the original Finite Element Method used in [1] while retaining the parallel memory distribution of [2]. The radiation field in x and y is now described fully including the 'fast' phase variations rather than via a complex envelope description. The code utilizes only open-source routines.

THE MODEL

An unnormalized vector basis:

$$\hat{\mathbf{f}} = f_x \hat{\mathbf{x}} + i f_y \hat{\mathbf{y}} \qquad (1)$$

is used to define a variable polarized undulator field

$$\mathbf{B}_w = \frac{B_w}{2}(\hat{\mathbf{f}} e^{-ik_w z} + c.c.) \qquad (2)$$

where B_w is the peak magnetic field strength so that f_x and f_y describe the strength of the wiggler magnetic field in x and y. The vector basis $\hat{\mathbf{f}}$ is un-normalized so that the RMS

magnetic field $\bar{B}_w$ varies from $B_w/\sqrt{2} \leq \bar{B}_w \leq B_w$ as the wiggler changes from planar to helical.

The electromagnetic field is defined as:

$$\mathbf{E}(x, y, z, t) = \frac{1}{\sqrt{2}} \left(\hat{\mathbf{e}} \xi_0 e^{i(kz - \omega t)} + \hat{\mathbf{e}}^* \xi_0^* e^{-i(kz - \omega t)} \right) \qquad (3)$$

with complex envelope $\xi_0(x, y, z, t)$ and the normalized vector basis $\hat{\mathbf{e}} = \frac{1}{\sqrt{2}}(\hat{\mathbf{x}} + i\hat{\mathbf{y}})$ is defined with $\hat{\mathbf{e}} \cdot \hat{\mathbf{e}} = \hat{\mathbf{e}}^* \cdot \hat{\mathbf{e}}^* = 0$ and $\hat{\mathbf{e}} \cdot \hat{\mathbf{e}}^* = 1$.

The 3D FEL is described using the coupled Maxwell-Lorentz equations which in the Compton limit and with the paraxial approximation gives:

$$\nabla^2 \mathbf{E} - \frac{1}{c^2} \frac{\partial^2 \mathbf{E}}{\partial t^2} = -\frac{\mu_0 e}{m} \sum_{j=1}^{N} \frac{\mathbf{p}_j}{\gamma_j} \delta^3(x_j, y_j, z_j) \quad (4)$$

$$\mathbf{F} = -e(\mathbf{E} + \mathbf{v} \times \mathbf{B}), . \qquad (5)$$

where $\delta^3(x_j, y_j, z_j) = \delta(x - x_j(t))\delta(y - y_j(t))\delta(z - z_j(t))$.

Projecting the wave equation (4) onto $\hat{\mathbf{e}}^*$ gives:

$$\left(\nabla^2 - \frac{1}{c^2} \frac{\partial^2}{\partial t^2} \right) E_\perp = -\frac{\mu_0 e}{m} \sum_{j=1}^{N} \frac{p_{\perp j}}{\gamma_j} \delta^3(x_j, y_j, z_j) \quad (6)$$

where $E_\perp = \xi_0 e^{i(kz - \omega t)} = E_x - iE_y$ is the transverse field. Similarly $p_{\perp j} = p_{xj} - ip_{yj}$ is the perpendicular momentum of the jth electron.

Defining the independent variables $\bar{z} = 2k_w \rho z$ and $\bar{z}_2 = 2k_w \rho \bar{\beta}_z(ct - z)/(1 - \bar{\beta}_z)$, equation (6) becomes:

$$\nabla_\perp^2 E_\perp + (2k_w \rho)^2 \left(\frac{\partial}{\partial \bar{z}} \left(\frac{\partial}{\partial \bar{z}} - \frac{2\bar{\beta}_z}{1 - \bar{\beta}_z} \frac{\partial}{\partial \bar{z}_2} \right) \right) E_\perp =$$

$$-\frac{e}{\epsilon_0 mc} 4k_w^2 \rho^2 \left(\frac{\bar{\beta}_z}{1 - \bar{\beta}_z} \right)^2 \frac{\partial}{\partial \bar{z}_2} \sum_{j=1}^{N} \frac{p_{\perp j}}{\beta_{zj} \gamma_j} \delta^3(x_j, y_j, \bar{z}_{2j}) \qquad (7)$$

and the independent variable of the parameters of the δ^3 Dirac delta function is now $\bar{z}$.

Assuming:

$$\left| \frac{\partial}{\partial \bar{z}} E_\perp \right| << \left| \frac{\bar{\beta}_z}{1 - \bar{\beta}_z} \frac{\partial}{\partial \bar{z}_2} E_\perp \right|, \qquad (8)$$

which is equivalent to the neglect of the backwards

wave [3], then the wave equation (7) simplifies to:

$$\nabla_\perp^2 E_\perp - (2k_w\rho)^2 \frac{2\bar{\beta}_z}{1-\beta_z}\frac{\partial E_\perp}{\partial\bar{z}\partial\bar{z}_2} =$$

$$-\frac{e}{\epsilon_0 mc}4k_w^2\rho^2\left(\frac{\bar{\beta}_z}{1-\bar{\beta}_z}\right)^2\frac{\partial}{\partial\bar{z}_2}\sum_{j=1}^{N}\frac{p_{\perp j}}{\beta_{zj}\gamma_j}\delta^3(x_j,y_j,\bar{z}_{2j}) \tag{9}$$

Projecting the Lorentz equation (5) onto $\hat{e}^*$ and changing to the variables $(\bar{z},\bar{z}_2)$ the equation for the transverse momentum is obtained:

$$\frac{dp_{\perp j}}{d\bar{z}} = \frac{-e}{2k_w\rho c\beta_{zj}}\Big[\xi_0 e^{-i\frac{\bar{z}_{2j}}{2\rho}} -$$

$$\frac{p_{zj}}{\gamma_j m}\Big(\frac{\xi_0}{c}e^{-i\frac{\bar{z}_{2j}}{2\rho}} + iB_wG^*\Big)\Big] \tag{10}$$

and the z component is:

$$\frac{dp_{zj}}{d\bar{z}} = \frac{-ep_{\perp j}}{4mck_w\rho\gamma_j\beta_{zj}}\Big(\frac{\xi_0^*}{c}e^{i\frac{\bar{z}_{2j}}{2\rho}} - iB_wG\Big) + c.c., \tag{11}$$

where $G = (f_x\cos(\bar{z}/2\rho) + if_y\sin(\bar{z}/2\rho))$ is a term describing electron 'jitter' motion in z resulting from propagation in a non-helical wiggler field. Using relation (11) with the equation for the electron energy:

$$\frac{dp_{zj}}{d\bar{z}} = mc\frac{d}{d\bar{z}}(\gamma_j\beta_{zj}),$$

along with equations (9), (10) and (11) and the scaling of [1], modified slightly so that:

$$\epsilon Q_j = \frac{1-\beta_{zj}}{\beta_{zj}}, \qquad\qquad \epsilon = \frac{1-\bar{\beta}_z}{\bar{\beta}_z},$$

$$\bar{x} = \frac{x}{\sqrt{l_g l_c}}, \qquad\qquad \bar{y} = \frac{y}{\sqrt{l_g l_c}},$$

$$\bar{p}_\perp = \frac{p_\perp}{mc}, \qquad\qquad A = \frac{e\sqrt{f_x^2+f_y^2}}{mc\omega_p\sqrt{2\gamma_r\rho}}$$

gives the final set of working equations which are solved numerically by the code:

$$-i\rho\left(\frac{\partial^2 A_\perp}{\partial\bar{x}^2} + \frac{\partial^2 A_\perp}{\partial\bar{y}^2}\right) + 2i\rho\frac{\partial^2 A_\perp}{\partial\bar{z}\partial\bar{z}_2} =$$

$$\sqrt{\frac{f_x^2+f_y^2}{2}}\frac{\gamma_r}{\bar{a}_w\bar{n}_p}\frac{\partial}{\partial\bar{z}_2}\sum_{j=1}^{N}\frac{\bar{p}_{\perp j}}{(1+|\bar{p}_{\perp j}|^2)^{1/2}}\times$$

$$(\epsilon Q_j(\epsilon Q_j+2))^{1/2}\delta^3(\bar{x}_j,\bar{y}_j,\bar{z}_{2j}) \tag{12}$$

$$\frac{d\bar{p}_{\perp j}}{d\bar{z}} = \frac{\bar{a}_w}{\rho\sqrt{2(f_x^2+f_y^2)}}\times$$

$$\Big(iG^* - \epsilon Q_j\Big(\frac{2\gamma_r\rho}{\bar{a}_w}\Big)^2 A_{\perp j}\Big) + F_j \tag{13}$$

$$\frac{dQ_j}{d\bar{z}} = \frac{\bar{a}_w}{4\rho}\sqrt{\frac{2}{f_x^2+f_y^2}}\frac{Q_j(\epsilon Q_j+2)}{1+|\bar{p}_{\perp j}|^2}\times$$

$$\Big(-i(\epsilon Q_j+1)(\bar{p}_{\perp j}G - \bar{p}_{\perp j}^*G^*)+$$

$$\epsilon Q_j\Big(\frac{2\gamma_r\rho}{\bar{a}_w}\Big)^2(\bar{p}_\perp A_{\perp j}^* + \bar{p}_{\perp j}^* A_{\perp j})\Big) \tag{14}$$

$$\frac{d\bar{z}_{2j}}{d\bar{z}} = Q_j \tag{15}$$

$$\frac{d\bar{x}_j}{d\bar{z}} = \sqrt{\frac{Q_j(2+\epsilon Q_j)}{1+|\bar{p}_{\perp j}|^2}}\Re(\bar{p}_{\perp j}) \tag{16}$$

$$\frac{d\bar{y}_j}{d\bar{z}} = -\sqrt{\frac{Q_j(2+\epsilon Q_j)}{1+|\bar{p}_{\perp j}|^2}}\Im(\bar{p}_{\perp j}) \tag{17}$$

where the equations for the $\bar{x}$, $\bar{y}$ and $\bar{z}_2$ electron coordinates are simply derived from the scaled momentum/energy relations. The field term $A_\perp = A_x - iA_y$ is the scaled perpendicular field, related to the scaled complex envelope A by $A_\perp = Ae^{-i\frac{\bar{z}_2}{2\rho}}$. Hence the code now solves explicitly for the $\bar{x}$ and $\bar{y}$ radiation field components. This assists in resolving some numerical issues requiring many conversions between real and complex numbers when the electrons interact with a complex envelope A.

The term F_j describes a generic focussing channel of the electron transverse motion. This is similar to the natural focussing of the helical wiggler which for convenience may be varied independently of the actual undulator used via a scaling factor f. In the scaled notation used here the focussing force is given by:

$$F_j = -f\frac{\beta_{zj}\bar{a}_w^2\sqrt{\epsilon}}{8\gamma_j\rho^2}(\bar{x}_j - i\bar{y}_j). \tag{18}$$

COMPUTATIONAL SOLUTION

The code integrates the working equations by using a split step Fourier method [4], where the first half step solves field diffraction in the absence of the electron transverse current and the second step propogates the electrons and field equation in the absence of diffraction. Where previously the code solved the non-diffractive half-step in Fourier space, as outlined in [2], it is now solved using a Finite Element Method [5]. However, the beneficial memory and processing distribution across processors in the parallel algotithm of the previous Fourier method is retained.

The resolution of the model is not limited to the resonant radiation wavelength. The field must be sampled on the sub-wavelength scale to describe the resonant wave oscillations to the desired resolved frequency. Because of this, the data sizes for a full 3D field and 6D electron phase-space distribution can be large, hence the use of a parallel code algorithm to distribute the data and solve the equations.

The code of [2] used a fully distributed memory solution which solved both field source and diffraction in the Fourier domain. In terms of memory distribution this

works well, however the solution requires a prohibitive number of calculations per step. In order to drive the Fourier field each electron must interact with *every* field node, and the number of calcuations required is then proportional to the number of electrons $\times$ the number of Fourier nodes. In a full 3D system (and with electrons in 6 dimensions), this can give the order of 10^{14} interactions per quarter step using a standard Runge Kutte 4th order method for a moderately sized system, each of which is composed of many computational operations. The base number of calculations for a moderate simulation is prohibitively inefficient.

In replacing the Fourier method with the finite element method, however, each electron interacts with only its 8 surrounding nodes, so the number of calculations is proportional to the number of electrons $\times 8$. The base number of calculations is therefore significantly smaller and the code runs much more efficiently.

The main problem with a parallel algorithm for this finite element model is in the uniform distribution of the data. There are two different interaction systems, the electrons and the field, which are constantly shifting spatially in time with respect to each another due to the slippage of the field with respect to the electrons. Any given electron must have its local field stored on its processor for any given step. However, the local field shifts with each step. Furthermore, the rate at which the local field shifts is not a constant in an unaveraged system - the equations allow the electron to have a rapid change in energy within one radiation period e.g. for very high radiation fields.

One approach is to pick one of the systems, either the field or electrons, distribute it evenly and fix this distribution. The data distribution for the other system must be calulated at each step and will be shifted around the processors as appropriate. If the field is chosen as the fixed distribution, the electron variables will be shifted between processors. However, this leads to a poor spread of the computational load, as the electrons can only generate, amplify, and interact with the field finite elements which immediately surrounds them. This is especially true for short electron bunches, which is one of the areas an unaveraged code is particularly useful - the electrons in the bunch will only be distributed over a small percentage of the processors available at any one time. Those processors will be doing all the work to drive the field. Taking the opposite approach, by distributing the electron data uniformly across the processors, the computational load is well spread. However, the management of the field data between processors can become complicated by the need for the electrons on one processor to interact with potentially distant field nodes and the desire to uniformly distribute the field nodes across processors for the diffractive half-step.

In the compromise of the code presented here, the electrons are distributed evenly in memory *and* a full copy of the field is kept on each processor. This is justified by considering the relative memory sizes for a typical FEL system: each electron has 6 dimensions and the number
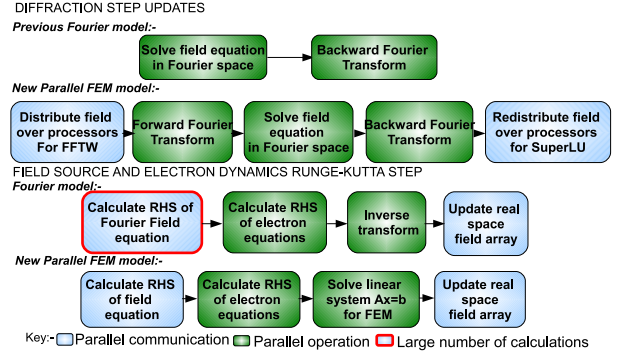

Figure 1: Illustration of the the differences in computational solution between [2] and the code used here.

of electrons can potentially be a few orders of magnitude larger than the number of field nodes; the field has only 3 dimensions. Clearly, the priority is to distribute the electrons in memory. However, recalculating the field distribution each step can add significant inter-processor communication time, which can hamper the ability of a parallel code for large processor numbers.

3D BEAM EFFECTS

The effects of the 3D electron beam are illustrated with a simple example. The beam is said to be matched when its radius is matched to the undulator focussing channel which may be calculated from the normalised emittance relation $\gamma\epsilon_x = \gamma\epsilon_y = \epsilon_n = \gamma r_b^2/\beta$ [6], and in terms of the scaled notation and putting in terms of the normalised emittance ϵ_n,

$$\bar{\sigma}_b = \left(\frac{2\sqrt{2}\rho\epsilon_n}{\epsilon \bar{a}_w l_g} \right)^{\frac{1}{2}} \qquad (19)$$

where l_g is the gain length of the FEL, and $\bar{\sigma}_b$ is the Gaussian radius in $\bar{x}$ and $\bar{y}$.

A simulation to test the beam matching effects was performed. The parameters used were

$$\rho = 0.015, l_b = 4l_c, \epsilon_n = 10^{-6}\mu\,m, \bar{a}_w = 1.5,$$
$$f_x = f_y = 1, \gamma_r = 489, \lambda_w = 0.03m,$$

and electron beam shot noise is simulated via the method of [7]. The beam radius should therefore be ≈ 1.61. The field evolution and interaction is artificially switched off, so the electrons travel unpeturbed through the wiggler. This allows the effect of only the focussing term on the electron motion to be observed.

The result is shown in figure 2. The matched beam radius is calculated by the code and the particles are then loaded according to the shot-noise model of [7]. It is seen that the noise introduces a small deviation from the matched beam radius giving a value of ≈ 1.56. The electron beam radius then exhibits a very small oscillation on
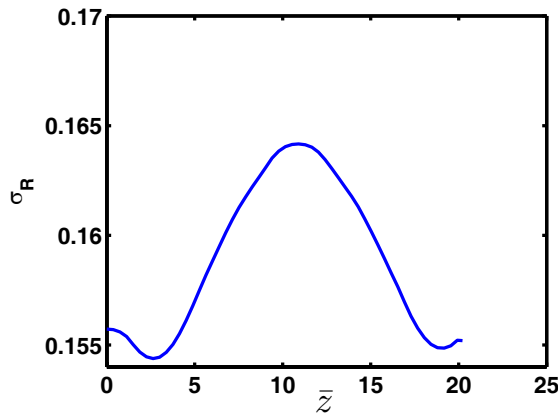
Figure 2: The radius of the electron beam as a function of propagation distance through the wiggler $\bar{z}$.
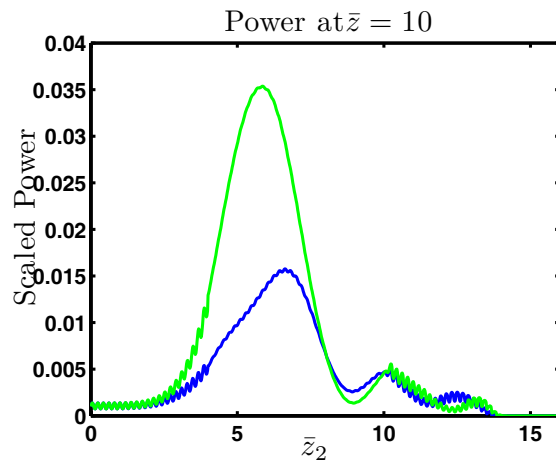

Figure 3: Power as a function of $\bar{z}_2$ after ≈ 10 gain lengths through the wiggler. Both simulations were run with identical parameters, one with emittance and beam focussing (blue) and one without (green).

propagating through the wiggler. Increasing the number of macroparticles will decrease this small noise-oscillation.

A simulation including self consistent electron-field interaction is now shown. The electrons are seeded by a field with a constant gaussian profile in the tranverse plane. The scaled rms radius of the seed radiation intensity is chosen to match the rms value of the gaussian distribution of the electron beam $\bar{\sigma}_r = \bar{\sigma}_b$. Radiation diffraction was artifically switched off for this example. This will therefore show only the effects of the 3D electron beam on the system. The electron beam parameters are the same as for the previous example, the seed field peak intensity in $\bar{x}$ and $\bar{y}$ is chosen so that the scaled power is 10^{-3}. For comparison, simulations are performed both with and without the emittance and focussing. The results are shown in Fig. 3. For the case of no emittance or focussing the beam transverse monmentum has zero spread and therefore does not diverge even without a focussing channel. For the case with emittance and focussing the beam is matched and retains a constant radius as shown above. Hence any effects in the generation of radiation can be attributed to emittance and betatron effects only. The expected reduction in power generated and rate of the instability are clearly seen.

CONCLUSIONS

A new model for describing a 3D variably polarized FEL has been presented which uses an efficiently parallelised algorithm with finite elements to solve the working equations. A simple example of matching a 3D electron beam to a focussing channel and a diffraction-free FEL interaction were shown. The new code uses only publically available linear-solvers etc. and is intended for open-source release in the near future. A post processing visualization package is being worked on. The method of modelling diffraction is currently being updated from the method of [2] which utilized a complex envelope A to describe the radiation field. The new model uses the full field of the radiation i.e. including the fast oscillatory variations.

REFERENCES

[1] C.K.W. Nam, P. Aitken and B.W.J. McNeil, Unaveraged Three Dimensional Modelling of the FEL, Proceedings of FEL 2008, Gyeongju, Korea

[2] L.T. Campbell and B.W.J. McNeil, A Fully 3D Unaveraged, Non-localised Electron, Parallelized Computational Model of the FEL, Proceedings of FEL 2009, Liverpool, UK

[3] B.W.J. McNeil and G.R.M. Robb, Phys. Rev. E **65**, 046503 (2002)

[4] R.H. Hardin and F.D. Tappert, *Applications of the split-step Fourier method to the numerical solution of nonlinear and variable coefficient wave equations*, SIAM Review, **15**, 423 (1973)

[5] K.H. Huebner, E.A Thornton and T.G. Byrom, *The Finite Element Method For Engineers*, Wiley (1995)

[6] R. Bonifacio R. Corsini et al, Rivista Del Nuovo Cimento Vol 15 N 11 (1993)

[7] B.W.J. McNeil M.W. Poole and G.R.M. Robb, Phys. Rev. ST - Acc. Beams **6**, 070701 (2003)